Published in final edited form as:
J Magn Reson Imaging. 2009 April ; 29(4): 917–923. doi:10.1002/jmri.21733.

CE-MRA of the Lower Extremities using HYPR Stack-of-Stars

Yan Wu, PhD[1], **Frank R. Korosec, PhD**[2,3], **Charles A. Mistretta, PhD**[2,3], and **Oliver Wieben, PhD**[2]

[1] Department of Electrical and Computer Engineering, University of Wisconsin – Madison

[2] Department of Medical Physics, University of Wisconsin – Madison

[3] Department of Radiology, University of Wisconsin – Madison

Abstract

Purpose—To investigate the properties of HYPR (HighlY constrained back PRojection) processing - the temporal fidelity and the improvements of spatial/temporal resolution - for contrast-enhanced MR angiography in a pilot study of the lower extremities in healthy volunteers.

Methods—HYPR processing with a radial 3D stack-of-stars acquisition was investigated for contrast-enhanced MR angiography of the lower extremities in 15 healthy volunteers. HYPR images were compared with control images acquired using a fast, multiphase, 2D Cartesian method to verify the temporal fidelity of HYPR. HYPR protocols were developed for achieving either a high frame update rate or a minimal slice thickness by adjusting the acquisition parameters. HYPR images were compared with images obtained using 3D TRICKS, a widely used protocol in dynamic 3D MRA.

Results—HYPR images showed good temporal agreement with 2D control images. In comparison with TRICKS, HYPR stack-of-stars demonstrated higher spatial and temporal resolution. High radial undersampling factors for each time frame were permitted, typically about 50 to 100 compared with fully sampled radial imaging.

Conclusion—In this feasibility study, HYPR processing has been demonstrated to improve the spatial or temporal resolution in peripheral CE-MRA.

Keywords

HYPR; radial acquisition; rapid imaging; contrast-enhanced MR angiography; lower extremities

Introduction

In dynamic imaging applications, 3D MRI is challenged to simultaneously provide high spatial and temporal resolution. Various techniques have been proposed for spatial, temporal, and spatio-temporal undersampling to improve the otherwise limited achievable resolution in one or both domains. For example, keyhole imaging (1), view sharing (2), and 3D TRICKS (3) update k-space regions at different rates and/or share k-space regions among multiple time frames. Parallel imaging approaches that make efficient use of coil arrays (4,5) have been used for dynamic imaging with increased frame rates but at the expense of a reduced signal-to-noise ratio (SNR). Undersampled volumetric radial imaging methods, such as undersampled stack-of-stars (6), PR-TRICKS (7,8) and VIPR (9), have

Corresponding Author: Oliver Wieben, PhD, Depts. of Medical Physics and Radiology, University of Wisconsin – Madison, Wisconsin Institutes for Medical Research, 1111 Highland Ave., Room L1316, Madison, WI 53705-2275, Telephone: 608-263-0793, Fax: 608-265-9840, Email: owieben@wisc.edu.

been used as an alternative trajectory to reduce the number of acquired projections while maintaining artifacts at acceptable levels. K-space weighting methods such as the KWIC method (10) and iterative optimization schemes (11) have been developed to further reduce streak artifacts in dynamic applications. MR angiography of the lower extremities requires broad right-left and superior-inferior coverage to include both legs simultaneously but far less anterior-posterior coverage. Therefore, the hybrid 3D PR stack-of-stars trajectory (6) is better suited for this application than the true 3D PR acquisition VIPR (9), which covers a spherical volume. In the 3D stack-of-stars method, radial sampling is applied in-plane and conventional phase encoding is used in the slice-encoding direction.

Recently, the HYPR (HighlY constrained back PRojection) concept was introduced as a reconstruction technique for radial acquisitions that exploits spatio-temporal correlations in dynamic datasets (12). HYPR processing is partially inspired by other approaches that exploit the redundancy of information in imaging sequences (13–15), here with a backprojection method. HYPR uses information from multiple undersampled time frames to form reference (composite) images, and uses these images to constrain the backprojection of temporally-weighted data from single time frames. Thereby, even faster frame rates than with previously reported dynamic radial undersampling methods (10,11) can be achieved in imaging situations with high spatio-temporal correlations, such as in CE-MRA.

This pilot study explores the use of HYPR for obtaining contrast-enhanced MR angiographic images of the lower extremities to improved temporal or spatial resolution beyond the current approaches. Volunteer studies were conducted to investigate the properties of HYPR, identify suitable imaging parameters, and validate image quality and waveform fidelity for vascular enhancement. Therefore, dynamic 2D Cartesian and 3D TRICKS angiograms were also acquired for performance evaluation and comparison.

Methods

3D Stack-of-Stars Acquisition

For the 3D stack-of-star acquisition, all z-phase encodings were acquired at one projection angle before the next projection angle is acquired to facilitate the inclusion of any number of projections in a time frame image. In the dynamic acquisition, each time frame consists of a set of projections that sparsely and almost uniformly covers the circular k-space plane. Different radial lines are sampled in subsequent time frames so that projections from several consecutive time frames can be combined to produce a composite image. The well-sampled composite images have high SNR and very few undersampling artifacts.

A key element for such an ordering scheme is the even distribution of projection angles in each undersampled time frame and composite image. As recently shown (16), an uneven distribution of projection angles degrades image quality. Here, we use the bit-reverse projection ordering, which is a 1D quasi-random sequence (17,18) with a base of 2, over the full set of projection angles. With this approach, the number of projections per time frame and per composite image can be retrospectively selected while an almost even distribution of projection angles is maintained. In our experience, the bit-reverse view ordering performed better than the golden ratio approach (16) in this application with few projections per time frame.

HYPR Reconstruction

In HYPR processing, information from several consecutive time frames is combined into a composite image that has compromised temporal resolution but high SNR and reduced artifacts. Consecutively, profiles from an individual time frame are reconstructed using the constraint that temporal information is deposited only in the vessel locations defined by the

composite image with spatial weighting provided by the composite image, as introduced in (12).

The HYPR reconstruction can also be regarded as the multiplication of a composite image by a weighting image which is produced from the highly-undersampled time frame data (normalized profiles) using unfiltered backprojection and provides high temporal resolution. Unfiltered backprojection is used to avoid the severe streak artifacts and low SNR that would otherwise come with the filtered backprojection. In the normalization of profiles, numerical instability from division by near-zero values must be avoided. A threshold was set at 5 percent of the maximum intensity of the projection values derived from a given composite image.

The composite image with high spatial resolution was formed by combining data from several consecutive frames surrounding the current time frame and applying standard filtered backprojection to the more densely populated data sets. The number of time frames combined to produce the composite image is referred as composite window width.

In Vivo Studies

Using 3D HYPR stack-of-stars, contrast-enhanced MR angiograms were obtained in 15 healthy volunteers (8 males, 7 females, age: 20 to 47 years) in different parts of the lower extremities (thighs, calves, or feet). All data were acquired on a clinical 1.5 T system (GE Healthcare, Waukesha, WI). The acquisition was such that a mask data set was acquired before the arrival of the bolus to allow for the subtraction of non-enhancing background tissues. A dose of 0.1–0.15 mmol/kg of a Gadolinium-based contrast agent (Omniscan, GE Healthcare, London, UK) was injected at a rate of 2 ml/s. Every volunteer received 2 or 3 injections in a study with a maximal dose of 0.3 mmol/kg.

The protocol for HYPR stack-of-stars method was adopted to achieve either high frame update rates or high spatial resolution, especially in the through-plane direction. Representative parameters for the coronal acquisitions with a spoiled gradient echo (SPGR) sequence were 24–64 slices, uninterpolated slice thickness = 0.8–3.0 mm, FOV = 24–44 cm, flip angle of 30 deg. Fractional echoes were acquired with either 160, 196, or 312 samples per readout, resulting in reconstructed images of 256 × 256, 320 × 320 or 512 × 512 data points, respectively. With a receiver bandwidth of ±62.5 kHz, the TE was 1.0–1.4 ms, and the TR was 3.4–6.7 ms. Based on results from related work (19), we limited the parameter space for this study by choosing 8 to 16 projections per time frame since fewer projections resulted in insufficient information on the spatial distribution of the signal and more projections extended the frame duration beyond what was considered desirable to capture challenging pathology such as dynamic filling patterns. The composite window width was 16 time frames, which was identified as a good compromise between SNR, artifact suppression, and accurate representation of the temporal evolution.

For 5 volunteers, a fast, multiphase, 2D Cartesian spoiled gradient echo sequence was also acquired to validate the temporal accuracy of HYPR. A thick coronal slice was prescribed to encompass the same volume covered by the corresponding HYPR stack-of-stars acquisitions. A spatial saturation pulse applied superior to the FOV reduced the inflow-induced signal variations caused by cardiac pulsatility. The sampling matrix was 256 × 128, and the TR and TE were 3.5 ms and 1.1 ms, respectively. Other acquisition parameters were identical to those used for the corresponding HYPR stack-of-stars acquisitions.

For 7 volunteers, a series of angiogram was acquired with the 3D Cartesian TRICKS sequence in order to compare the HYPR stack-of-stars method with the standard clinical protocol used for peripheral CE-MRA at our institution: acquired in-plane matrix = 196 ×

180, reconstructed matrix = 320 × 224, partial field-of-view acquisition (80% in phase-encoding direction), TR/TE = 4.2/1.1 ms, other acquisition parameters were identical to the HYPR stack-of-stars acquisitions.

For image display and evaluation, maximum intensity projection (MIP) images were formed from the source images. The signal intensities within a region of interest (ROI) were measured in the MIP images for 3D acquisitions or the 2D images for 2D acquisition. Time curves obtained from a HYPR series were evaluated for temporal accuracy (compared with corresponding 2D acquisitions) and improvements in temporal resolution (compared with corresponding TRICKS).

Results

Figure 1 shows a comparison of single time frame images reconstructed using HYPR and conventional filtered backprojection from a calf exam. Reconstructed images have an in-plane matrix of 512 × 512 (with a fractional echo length of 312 data points acquired along each radial line) and a slice thickness of 1.6 mm. Each time frame was produced from 16 projections, representing a speedup factor of 50 relative to fully-sampled radial imaging (804 projections for full sampling/16 projections for the HYPR frame) and a speedup factor of 32 relative to conventional Cartesian imaging (512 phase encodings/16 projections for the HYPR frame). The frame update rate for HYPR is 4.3 sec, and the reconstruction window for the corresponding composite images spans 69 sec. The HYPR image displays much higher image quality than the filtered backprojection image in terms of improved SNR and reduced undersampling streak artifacts due to the benefits from the high-quality composite image. Please note that all HYPR images were reconstructed offline and have not been corrected for gradient nonlinearities, therefore appearing spatially distorted particularly towards the edges of large FOV acquisitions. The images can be easily corrected with the proper parameters for geometric corrections.

Figure 2 displays a series of HYPR images with high spatial resolution and high frame update rate, which were obtained from a foot exam. Relevant acquisition and reconstruction parameters were: 312 samples per radial k-space line (partial echo for 512 reconstructed points), 26 slices (zero-filled to 52) with an acquired slice thickness of 3.0 mm, a TR of 4.8 ms, a TE of 1.0 ms, and a FOV of 30 cm × 30 cm. Each time frame was produced using 16 projections. The composite images were produced using projections from 16 time frames, thereby spanning a reconstruction window of 30.4 sec. A single dose (0.1 mmol/kg) of a Gadolinium-based contrast agent was injected at a rate of 2 ml/sec. Every fifth frame is shown. In this example, the frame update time was 1.9 sec for HYPR. Thus, several time frames showing only arterial signal were obtained before the veins and the stationary tissues enhanced from the contrast agent.

Figure 3 illustrates the temporal accuracy of HYPR from another foot study. Images, as displayed in (a) and (b), were acquired using a 2D fast multiphase sequence and a HYPR scan. Relevant acquisition parameters in this study were: 75% fractional echo = 196 samples, 32 slices (zero-filled to 64), acquired slice thickness = 2.4 mm, TR/TE = 5.9/1.0 ms, FOV = 24 cm. A dose of 0.15 mmol/kg of Gadolinium-based contrast agent was injected at a rate of 2 ml/sec. Every eight projections were included in a time frame image. The corresponding signal intensity curves are compared in (c), which was measured from an ellipsoidal ROI placed in an artery in the series of MIP images (bold arrow). The HYPR curve closely tracks the true 2D curve even when the HYPR images are reconstructed using as few as 8 projections per time frame with a moderate composite window width of 16 time frames. This temporal fidelity of HYPR exists for other ROIs placed in arteries and veins. The time curve obtained from the composite images demonstrates poorer temporal

resolution because the composite images represent information that is averaged over multiple time frames. The plot in (d) demonstrates the HYPR signal intensity curves measured from ROIs placed in an artery and a vein in the midsection of the foot. With an achieved frame update time of 1.5 sec, the HYPR contrast curves of the artery and vein are well separated, which is particularly challenging in foot imaging due to the shorter circulation time. In this case, the reconstruction window for composite images is 24 sec.

Figure 4 shows calf images obtained using Cartesian TRICKS and the HYPR stack-of-stars method, demonstrating the improved temporal resolution of HYPR. Here, the reconstructed data matrix was 320 × 224 for TRICKS, and 256 × 256 for HYPR. HYPR images can be reconstructed using any number of projections per time frame from the acquired data set when the quasi-random scheme is applied to determine the order in which projections are acquired. Using 8 vs 16 projections per time frame, the normalized time curve obtained from the corresponding HYPR images closely tracks each other. HYPR images reconstructed using 8 projections per time frame provided a speedup factor of about 7 compared to TRICKS images, yielding a frame update time of 1.0 sec vs 7.1 sec, when similar spatial resolution, coverage, and image quality were achieved. The reconstruction window for the composite images is 16 sec with temporal averaging.

Alternatively, the gains in the frame update rate and SNR achieved using HYPR processing can be traded for improvements in spatial resolution, especially the through-plane resolution in the stack-of-stars acquisition. Figure 5 shows a side-by-side comparison of sagittal calf MIP images produced using coronal slice images from a TRICKS and a HYPR stack-of-stars acquisition. With HYPR, a much higher through-plane spatial resolution (0.8 mm vs 3.0 mm) was obtained while a similar frame update rate (6.9 sec vs 7.1 sec) is maintained.

Finally, Table 1 shows calf protocols that can be used to achieve high spatial resolution or high temporal resolution. Using the given parameters, a high spatial resolution can be obtained as high as $0.8 \times 0.8 \times 1.6\ mm^3$ (with a frame update time of 5.6 sec) in the former case, whereas in the latter case, a high temporal resolution can be obtained with a frame update time of 1.7 sec (for a spatial resolution of $1.7 \times 1.7 \times 3.0\ mm^3$). These protocols can be applied in more systematic/statistical clinical studies.

Discussion

In HYPR imaging, the composite images contain temporally-averaged information because they incorporate data from a reconstruction window with a wide temporal aperture. However, this temporal averaging effect in the composite images is compensated in the HYPR images by the corresponding weighting image. With proper imaging parameters, the preservation of arterial and venous enhancement patterns is demonstrated in the comparison of HYPR images with reference images obtained using a fast multiphase 2D sequence.

Challenging conditions that may limit the gains from HYPR processing include low sparsity and low spatial-temporal correlation in the image series. The temporal accuracy of HYPR can decrease when objects are very close to each other and their signal intensities change dramatically and asynchronously. These errors can be caused from “cross talk” of the objects through the unfiltered backprojection process in the weighting images which is characterized by a 1/r blurring kernel. This problem might be overcome by using an alternative filter to the unfiltered back projection operator as suggested for HYPR LR processing (20). Errors can also be introduced from inaccurate temporal information appearing in the composite image. Problems in these situations might be overcome by employing a narrower composite window. Iterative HYPR approaches such as CG-HYPR (21) or I-HYPR (22), which employ additional consistency criteria, can improve the

accuracy of HYPR processing. However, in CE MRA of the lower extremities, the sparsity and spatio-temporal correlation are fairly high. Thus, the signal enhancement waveforms obtained with HYPR closely tracked the time curves obtained from the fast multiphase 2D method, even when very few projections per time frame were used to form a time frame HYPR image. In these datasets, the use of iterative methods did not demonstrate apparent improvements in image quality or temporal waveforms. However in situations where the spatio-temporal correlation is low such as arteriovenous malformations (AVMs) in cranial imaging or differential fillings, or when images are densely populated or quantitative imaging is preferred such as in perfusion imaging, HYPR might benefit from such iterative processing.

The current *in vivo* studies in CE MRA of the lower extremities have been acquired in volunteers. Patient data might differ due to motion or complex enhancement of arteries and veins. In the presence of motion, the quality of composite images is reduced, and the iterative method mentioned above, I-HYPR, may be helpful. Based on the study of temporal accuracy in this study and other simulations we conducted (19), we do not anticipate significant inaccuracies in the temporal waveforms for differential filling patterns of the vessels.

The load for a HYPR reconstruction is significantly heavier as compared to a single volume CE MRA or more traditional dynamic imaging approaches. In order to minimize the reconstruction time and provide rapid feedback on the scan, the reconstruction algorithm was implemented on the standard GE MR reconstruction engine with parallel processing functionality, requiring about 10 minutes of processing time for our current peripheral MRA protocol (23).

The SNR in a HYPR image is dominated by the corresponding composite image, and thus is mostly determined by the number of projections per time frame and the composite window width. A wide composite window leads to high SNR, but may cause more severe temporal inaccuracies. For a fixed composite window width, a larger number of projections per time frame lead to higher SNR but reduced temporal resolution. There are tradeoffs between SNR, temporal resolution and temporal accuracy. In these *in vivo* CE MRA studies of the lower extremities, about 8 to 16 projections per time frame and a moderate composite window width of 16 time frames were sufficient to maintain good SNR in 512 × 512 images having a slice thickness of 1.0 mm. Using HYPR, the SNR benefit from the composite image can also be used to achieve high spatial resolution. In other techniques such as TRICKS and parallel imaging, the spatial resolution is limited not only by the concomitant reductions in frame update rate but also by SNR losses associated with increases in spatial resolution.

While HYPR parameters are still optimized for clinical applications, it is desirable to have the flexibility to adjust parameters such as the number of projections per time frame after data acquisition is completed. If the quasi-random scheme is applied to the interleaved set of projections, the retrospective selection of composite window width is facilitated, and there is no clustering of projections in composite images. If the quasi-random scheme is applied to the complete set of projections, the flexible reconstruction of HYPR images is enabled using any number of projections per time frame for a given data set, and there is no clustering of projections in both weighting images and composite images. The minimal permissible number of projections per time frame is determined by the conditions of sparsity and spatial-temporal correlation, which vary from application to application and from volunteer to volunteer. This quasi-random projection acquisition ordering scheme provides a practical solution to the proper selection of parameters, which is a challenging theoretical problem currently under investigation (24).

The improvements in temporal and spatial resolution and image quality offered by HYPR potentially provide improved diagnostic information. For example, the improved temporal resolution could allow for better differentiation of arteries and veins especially in areas affected by asynchronous filling. Improved spatial resolution in the slice-encoding direction reduces the anisotropy of the acquired voxel dimensions and might improve the characterization of pathology and identification of smaller vessels. Alternatively, HYPR could be possibly used to reduce the contrast dose.

In conclusion, we demonstrated in this *in-vivo* feasibility study of 15 volunteers that the HYPR imaging approach can be used to improve the spatial or temporal resolution in peripheral CE-MRA. High radial undersampling factors for each time frame were permitted, typically about 50 to 100 compared with fully sampled radial imaging. Using only a few projections per time frame, HYPR images contained good SNR and minimal undersampling artifacts, which were made possible through the use of the composite images during image reconstruction. Simultaneously, high temporal resolution with good temporal agreement with the true contrast-enhancement curves determined from fast 2D images was obtained through the incorporation of the weighting images. Two protocols were developed to maximize either temporal resolution or spatial resolution in the through-plane direction. These protocols will be investigated in subsequent patient studies.

Acknowledgments

This work was funded by NIH grants R21 EB006393-01 and R01 EB006882-01. We also gratefully acknowledge the support of GE Healthcare.

Grant Support: NIH grants R21 EB006393-01 and R01 EB006882-01

References

1. van Vaals JJ, Brummer ME, Dixon WT, et al. “Keyhole” method for accelerating imaging of contrast agent uptake. J Magn Reson Imaging. 1993; 3(4):671–675. [PubMed: 8347963]
2. Riederer SJ, Tasciyan T, Farzaneh F, Lee JN, Wright RC, Herfkens RJ. MR fluoroscopy: technical feasibility. Magn Reson Med. 1988; 8(1):1–15. [PubMed: 3173063]
3. Korosec FR, Frayne R, Grist TM, Mistretta CA. Time-resolved contrast-enhanced 3D MR angiography. Magn Reson Med. 1996; 36(3):345–351. [PubMed: 8875403]
4. Sodickson DK, Manning WJ. Simultaneous acquisition of spatial harmonics (SMASH): fast imaging with radiofrequency coil arrays. Magn Reson Med. 1997; 38(4):591–603. [PubMed: 9324327]
5. Pruessmann KP, Weiger M, Scheidegger MB, Boesiger P. SENSE: sensitivity encoding for fast MRI. Magn Reson Med. 1999; 42(5):952–962. [PubMed: 10542355]
6. Peters DC, Korosec FR, Grist TM, et al. Undersampled projection reconstruction applied to MR angiography. Magn Reson Med. 2000; 43(1):91–101. [PubMed: 10642735]
7. Vigen KK, Peters DC, Grist TM, Block WF, Mistretta CA. Undersampled projection-reconstruction imaging for time-resolved contrast-enhanced imaging. Magn Reson Med. 2000; 43(2):170–176. [PubMed: 10680679]
8. Du J, Carroll TJ, Brodsky E, et al. Contrast-enhanced peripheral magnetic resonance angiography using time-resolved vastly undersampled isotropic projection reconstruction. J Magn Reson Imaging. 2004; 20:894–900. [PubMed: 15503332]
9. Barger AV, Block WF, Toropov Y, Grist TM, Mistretta CA. Time-resolved contrast-enhanced imaging with isotropic resolution and broad coverage using an undersampled 3D projection trajectory. Magn Reson Med. 2002; 48(2):297–305. [PubMed: 12210938]
10. Song HK, Dougherty L. k-space weighted image contrast (KWIC) for contrast manipulation in projection reconstruction MRI. Magn Reson Med. 2000 Dec; 44(6):825–32. [PubMed: 11108618]

11. Liu J, Redmond MJ, Brodsky EK, et al. Generation and Visualization of Four-Dimensional MR Angiography Data Using an Undersampled 3-D Projection Trajectory. IEEE Trans Med Imaging. 2006; 25(2):148–156. [PubMed: 16468449]
12. Mistretta CA, Wieben O, Velikina J, et al. Highly constrained backprojection for time-resolved MRI. Magn Reson Med. 2006; 55(1):30–40. [PubMed: 16342275]
13. Tsao J, Boesiger P, Pruessmann KP. k-t BLAST and k-t SENSE: dynamic MRI with high frame rate exploiting spatiotemporal correlations. Magn Reson Med. 2003; 50(5):1031–1042. [PubMed: 14587014]
14. Huang Y, Wright G. Time-resolved MR angiogarphy with limited projections. Magn Reson Med. 2007; 58(2):316–25. [PubMed: 17654575]
15. Liang ZP, Madore B, Glover GH, Pelc NJ. Fast algorithms for GS-model-based image reconstruction in data-sharing Fourier imaging. IEEE Trans Med Imaging. 2003; 22(8):1026–1030. [PubMed: 12906256]
16. Winkelmann S, Schaeffter T, Koehler T, Eggers H, Doessel O. An optimal radial profile order based on the Golden Ratio for time-resolved MRI. IEEE Trans Med Imaging. 2007; 26(1):68–76. [PubMed: 17243585]
17. Morokoff WJ, Caflisch RE. Quasi-random sequences and their discrepancies. SIAM J Sci Comput. 1994; 15(6):1251–1279.
18. Bratley P, Fox BL, Niederfieiter H. Implementation and tests of low-discrepancy sequences. ACM Trans on Modeling and Computer Simulation. 1992; 2(3):195–213.
19. Wu Y, Korosec FR, Mistretta CA, Wieben O. Evaluation of Temporal and Spatial Characteristics of 2D HYPR Processing Using Simulations. Magn Reson Med. 2008; 59:1090–8. [PubMed: 18429029]
20. Johnson K, Velikina J, Wu Y, Kecskemeti S, Wieben O, Mistretta CA. Improved Waveform Fidelity Using Local HYPR Reconstruction (HYPR LR). Magn Reson Med. 2008; 59:456–62. [PubMed: 18306397]
21. Griswold, M.; Barkauskas, K.; Blaimer, M.; Moriguchi, H.; Sunshine, J.; Duerk, J. More optimal HYPR reconstructions using a combination of HYPR and conjugate-gradient minimization. Proceedings of the 18th Annual Meeting of the International MRA Club; Basel, Switzerland. 2006. p. 29
22. O'Halloran RL, Wen Z, Holmes J, Fain SB. Iterative projection reconstruction of time-resolved images using highly-constrained back-projection (HYPR). Magn Reson Med. 2008; 59:132–9.22. [PubMed: 18058939]
23. Carrillo, A.; Busse, RF.; Brittain, J.; Wieben, O.; Wu, Y.; Mistretta, CA.; Korosec, FR. Accelerated HYPR Reconstruction. 16th Proceedings of the ISMRM; Toronto, CA. 2008. p. 3146
24. Velikina, J.; Wu, Y.; Mistretta, CA. Prediction of HYPR performance based on image sparsity and spatio-temporal correlation. Proceedings of the 19th Annual Meeting of the International MRA Club; Istanbul, Turkey. 2007.

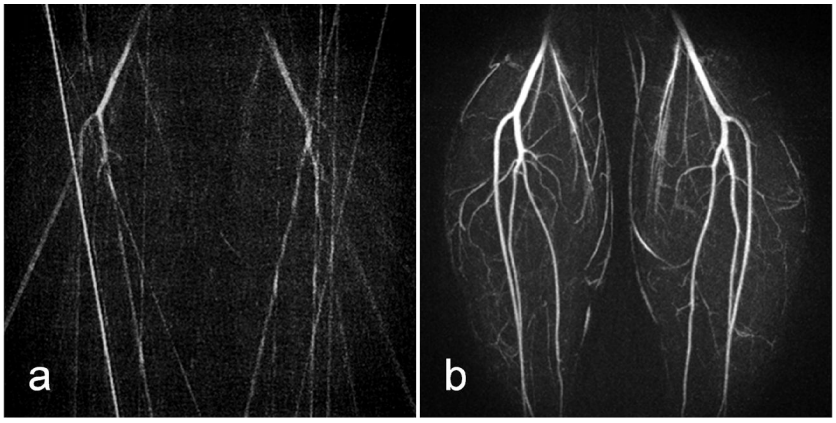

FIG. 1.

A single time frame from a calf exam reconstructed with standard filtered back projection (a) and HYPR (b). Both maximum intensity projection (MIP) images have an in-plane matrix of 512 × 512 and were formed using images that were reconstructed from 16 projections per time frame. The composite images used for the HYPR reconstruction were formed using projections from 16 time frames, which is largely responsible for the improvements in image quality.

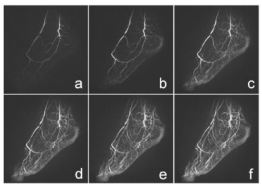

FIG. 2.

A series of maximum intensity projection (MIP) images obtained using HYPR for a foot exam. The frame update time is 1.9 s. Every fifth frame is displayed. Several time frames showing only arterial signal were obtained before the veins and the stationary tissues enhanced from the contrast agent.

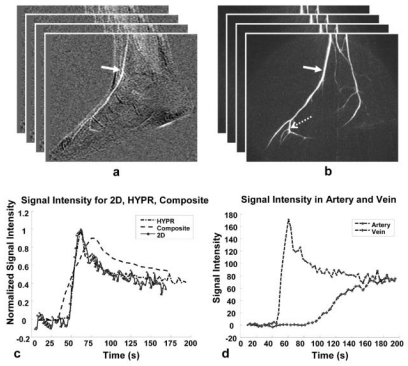

FIG. 3.

HYPR results from another foot exam in a healthy volunteer. From two successive contrast injections, images were acquired using a fast, multiphase, 2D Cartesian scan and a HYPR scan, as displayed in (a) and (b), respectively. A representative arterial signal curve obtained from a proximal ellipsoidal ROI analysis (bold arrow) is illustrated in (c). The HYPR curve closely tracks the true curve obtained from the 2D study, whereas the composite curve has a pronounced temporal averaging effect. The signal intensity curves measured from an artery and a vein in the midsection of the foot are plotted in (d). With a HYPR frame update time of 1.5 s, the contrast curves from the artery and vein are well separated.

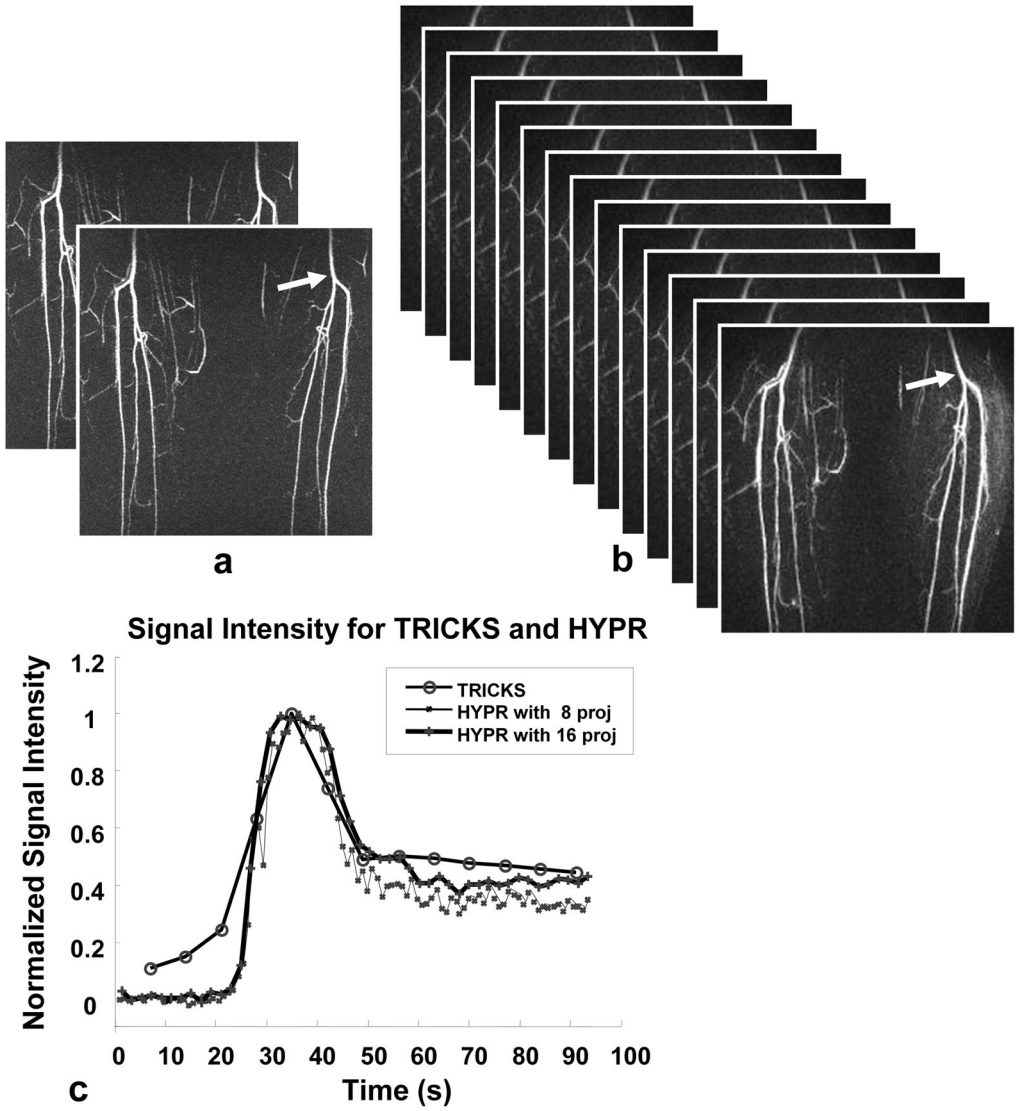

FIG. 4.

Representative calf study acquired using a TRICKS scan (a) and a HYPR scan reconstructed with 8 projections per time frame (b).. The normalized signal intensity curves obtained from a proximal ROI (arrow) with the corresponding TRICKS acquisition and stack-of-stars acquisition reconstructed using HYPR with 8 and 16 projections per time frame are shown in (c). The HYPR images reconstructed using 8 projections per time frame are updated 7 times faster than the TRICKS time frames.

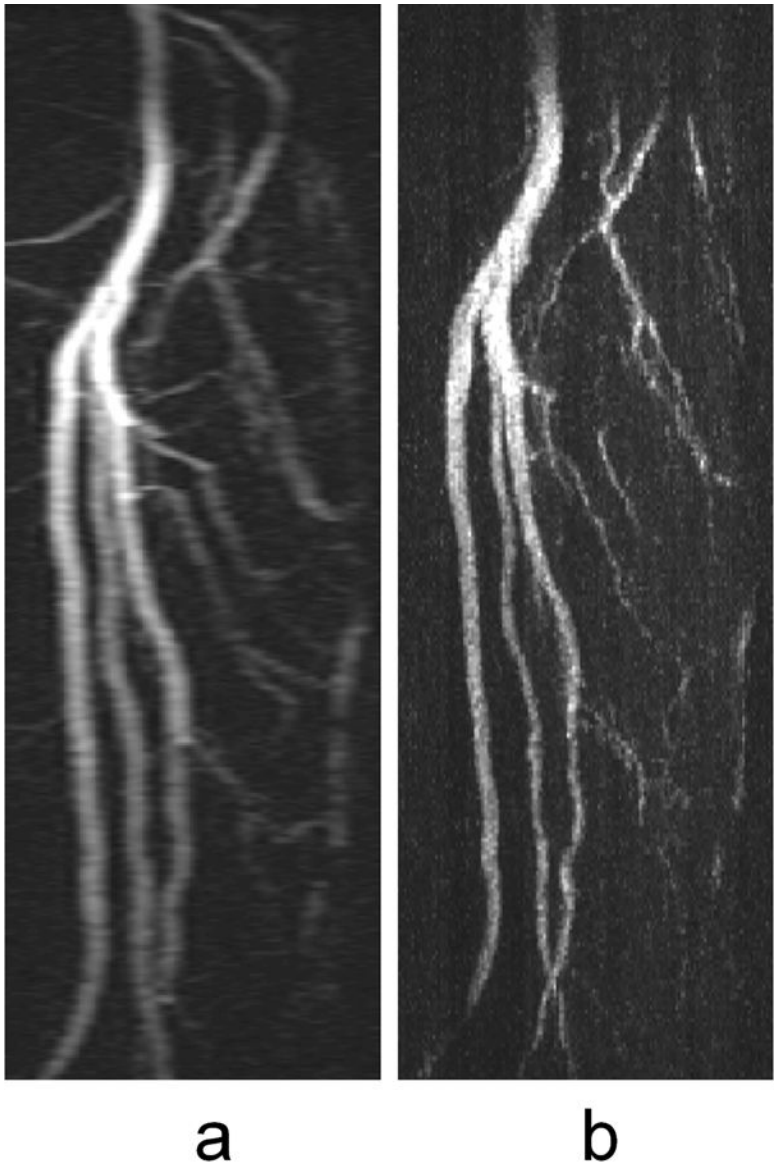

FIG. 5.

Sagittal maximum intensity projection (MIP) images of the vessels in the calves of a healthy volunteer acquired in the coronal plane using a TRICKS acquisition (a) and a HYPR acquisition (b) with similar frame update rates and in-plane resolution. HYPR processing made it possible to reduce the slice thickness from 3.0 mm for the TRICKS exam to 0.8 mm for the HYPR exam.

Table 1

Calf Protocol for High Spatial or High Temporal Resolution

	High Spatial Resolution	High Temporal Resolution
FOV (cm)	44	44
Matrix	512×512	256×256
In-plane resolution	0.8×0.8	1.7×1.7
Slice thickness(mm)	1.6/0.8	3.0/1.5
Number of slices	64 (ZIP to 128)	32 (ZIP to64)
TR/TE(ms)	5.5/1.2	3.4/1.0
Flip angle	30	30
Projections/frame	16	16
Composite width (frames)	16	16
Temporal resolution(sec)	5.6	1.7